

Transitional flow in intracranial aneurysms – a space and time refinement study below the Kolmogorov scales using Lattice Boltzmann Method

Kartik Jain ^{*1,2}, Sabine Roller¹, and Kent-André Mardal^{2,3}

¹*Simulation Techniques and Scientific Computing, University of Siegen, Hölderlinstr. 3, 57076 Siegen, GERMANY*

²*Center for Biomedical Computing, Simula Research Laboratory, N-1325 Lysaker, NORWAY*

³*Department of Mathematics, University of Oslo, 0316 Oslo, NORWAY*

Abstract

Most Computational Fluid Dynamics (CFD) studies of hemodynamics in intracranial aneurysms are based on the assumption of laminar flow due to a relatively low (below 500) parent artery Reynolds number. A few studies have recently demonstrated the occurrence of transitional flow in aneurysms, but these studies employed special finite element schemes tailored to capture transitional nature of flow. In this study we investigate the occurrence of transition using a standard Lattice Boltzmann method (LBM). The LBM is used because of its computational efficiency, which in the present study allowed us to perform simulations at a higher resolution than has been done in the context of aneurysms before. The high space-time resolutions of $8\ \mu\text{m}$ and $0.11\ \mu\text{s}$ resulted in nearly 1×10^9 cells and 9×10^6 time steps per second and allowed us to quantify the turbulent kinetic energy at resolutions below the Kolmogorov scales. We perform an in-depth space and time refinement study on 2 aneurysms; one was previously reported laminar, while the other was reported transitional. Furthermore, we investigate the critical Reynolds number at which the flow transitions in aneurysms under time constant inflow conditions.

keywords— intracranial aneurysm; Lattice Boltzmann Method; convergence; transitional flow

1 Introduction

Stroke caused by aneurysm rupture is a major cause of morbidity or mortality in the modern world⁴⁴. For instance, 3.5 – 5 % of the European population or nearly 18.5 million patients harbor aneurysms, and management of aneurysm patients amounts to 25 % of all stroke related costs, which is nearly 5.5 Billion Euro per year in EU nations⁹. A current and major challenge for aneurysm management lies in the estimation of risk of rupture in a patient-specific manner.

*Corresponding Author; E-mail: kartik.jain@uni-siegen.de; Phone: +49-271-740-3882

Recent image-based CFD studies have been successful in retrospectively classifying aneurysms according to the rupture status^{6;5;38;49;34;53}. The above mentioned studies are all based on the assumption of laminar flow because of the low Reynolds number (below 500) - an assumption that justifies the choice of methods and simulations with meshes in the order of a few hundred thousand to 5 million cells and time steps in the range of 100 to 4000 per cardiac cycle.

It is well-known that transition may occur for Reynolds numbers below 2000 (the transition threshold in pipe flow). In the context of intracranial aneurysms,⁴⁰ reported turbulence in idealized aneurysms glass models already at Reynolds number 500. Similarly,⁴⁶ investigated idealized glass models of bifurcations and the carotid siphon and found that the threshold for transition was 600 and 900, respectively.

Numerical investigations of fluctuations in physiological flows have been dominated by the use of finite volume method⁷ or spectral element methods³². Two recent computational studies demonstrate transitional flow in aneurysms^{50;51} - these studies employed low-order finite elements but the scheme was tailored to minimize numerical dissipation in order to capture transition. In the present study, we investigate whether standard Lattice Boltzmann methods are suitable for transition studies, in particular because these methods introduce numerical dissipation proportional to the time stepping^{29;30;33}.

Whereas numerical modeling can be efficiently utilized for the simulation of fully developed turbulent flows, the capture of the onset of transition in a flow poses additional challenges. Accurate simulation of transitional flows is accomplished when all the spatial and temporal scales of flow are numerically resolved - this technique is termed direct numerical simulation (DNS). Resolving the small structures (Kolmogorov microscales) in a turbulent flow requires computations of the order of Re^3 implying the suitability of DNS only for moderate Re flows. Blood is a suspension of plasma and blood cells but is modeled as a homogeneous fluid in our study, as is commonly done for hemodynamic computations in aneurysms. Treating blood as a continuum allow us to perform DNS and quantify the Kolmogorov scales from a fluid mechanical point of view within the modeling assumptions.

The goal of the present study is to investigate whether the Lattice Boltzmann Method (LBM) would reproduce the previously reported transition, and what would be the limit of resolutions until which there will be qualitative and quantitative changes in the flow. We discuss in the end about the role of such high resolutions in achieving *numerical convergence*.

To investigate convergence, we perform an in-depth refinement study on two selected aneurysms out of the 12 previously studied in⁵¹: one with laminar flow and the other with transitional flow. As⁵¹ we employ a constant inflow and Newtonian rheology of blood to facilitate an effective comparison. We analyze the convergence of velocity and WSS in the laminar case and compute Kolmogorov micro-scales and turbulent kinetic energy spectra in the transitional case. In addition, as^{6,4} suggest that flow complexity in terms of the number of or stability of vortices potentially provide improved analysis, we study the robustness of the so-called Q-criterion, which is an objective definition of vortices, developed for transitional/turbulent flows¹⁹. Finally, we explore the critical Reynolds number at which transition occurs in the transitional case and examine if the flow would transition in the laminar case upon increasing the parent artery Re to a value within physiologically acceptable range.

2 Methods

Computational meshes based on the surface meshes (STL) were created from the two out of 12 aneurysms in⁵¹ using the mesh generator *Seeder*¹⁵. One of the chosen models was reported to have laminar flow and the other showed transitional/unstable flow⁵¹. These models are shown in Figure 1 and referred to as Model A and B respectively in the following.

2.1 Models

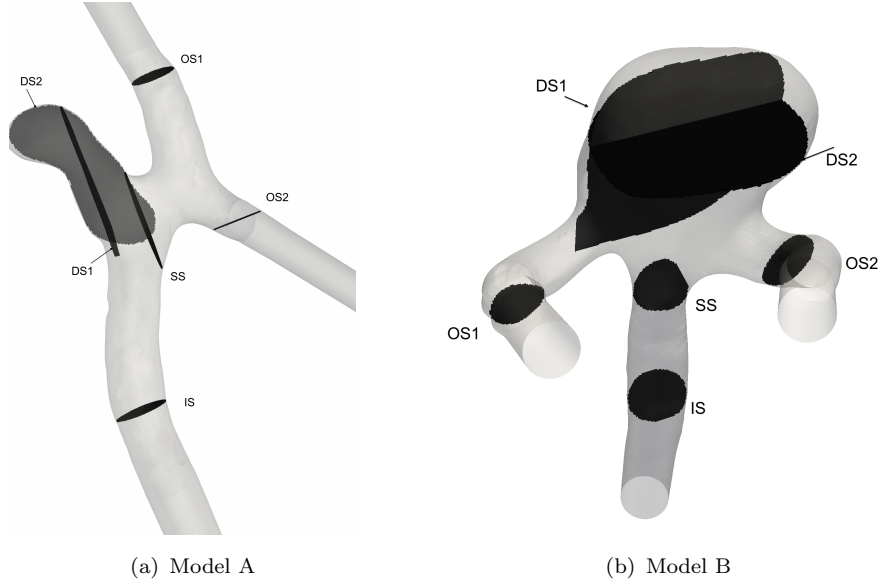


Figure 1: Two Middle Cerebral Artery (MCA) aneurysm models used in this study. The planes where flow quantities were computed are shown. IS: inlet slice, SS: saccular slice, DS1/DS2: Dome Slices, OS1/OS2: slices at each outlet

The inlets and outlets of the models were extended by 10 diameters to ensure the damping out of effects due to the boundary conditions. The initial conditions were set to zero velocity and pressure. The flow was allowed to develop for 2 initial seconds to wash away the initial transients. At the outlet a zero pressure extrapolation boundary condition was prescribed as described in²⁵. All the vascular walls were assumed to be rigid and the arbitrary curved surfaces were represented by a higher order no-slip boundary condition, which aligns the LBM velocity directions to the curved surfaces thereby compensating for the staircase approximation of boundaries in a LBM cartesian mesh³. The D3Q19 stencil was chosen in this study for LBM computations which describes 19 discrete velocity links per compute cell in 3 dimensions.

The blood rheology was represented with constant density and viscosity using a Newtonian description, i.e. $\rho = 1.025 \text{ g/cm}^3$ and $\nu = 0.035 \text{ Poise}$. A uniform parabolic velocity profile with a mean of $U = 0.5 \text{ m/s}$ was prescribed at the inlet, corresponding to peak systolic conditions at the MCA M1 segment²⁷ as was also done in⁵¹. This is represented by a bounce back rule in the LBM. The diameters of the parent artery of the aneurysms A and B were 2.24 and 2.41 mm respectively, resulting in parent artery Reynolds number of 328 and 351.

Velocity and WSS for Model A and B were analyzed for convergence in terms of both point-wise and average (plane area-weighted) quantities at the planes shown in

Figure 1. WSS is computed locally for each cell from the higher order moments of particle distribution functions in the LBM framework²⁸. The correction to staircase approximation accomplished by the higher order representation of the curved surface³ automatically results in a comparatively more accurate computation of WSS, as the correction is reflected in the distribution function.

High Performance Computations

The aneurysm models A and B were discretized with cubical cells of 128, 64, 48, 32, 16 and 8 μm sides. Table 1 lists the number of fluid cells, time step (δt) and the number of time steps per second ($1/\delta t$) for each aneurysm. The time step is coupled with the grid spacing in LBM as $\delta t \sim \delta x^2$, which reflects the *diffusive time scaling* necessary to recover the incompressible Navier-Stokes equation from the Lattice Boltzmann Equation²⁴. Errors in the LBM computations can be characterized by the lattice Mach number which, and the time step δt can be tuned by the relaxation parameter Ω which is the Bhatnagar-Gross-Krook (BGK) collision operator. It was set to $\Omega = 1.93$ in the present study - a value that keeps the lattice Mach number within the limits of stability³¹. We note that the coupling of Ω with lattice Mach number and the low Mach number limit in LBM would not allow us to simulate flow in these aneurysms at a resolution coarser than 128 μm . Further details concerning the influence of microscopic parameter Ω on macroscopic flow phenomena, and the association of LBM with Navier-Stokes equations can be found in^{31;24;39}.

The total number of cells with highest resolution of 8 μm was nearly one billion for Model B and 400 million for Model A due to the respective difference in the volumes of the two. The Lattice Boltzmann flow solver *Musubi*¹⁷ was used for simulations which is a part of the end-to-end parallel simulation tool chain - Adaptable Poly Engineering Simulator, *APES*^{43;26}. The verification and validation efforts for *Musubi* include comparison of results against benchmarks with analytical solutions^{16,17} as well as against laboratory experiments.²³ Validation for transitional flows in physiologically realistic geometries is specifically performed in.²⁰

$\delta x(\mu\text{m})$	$\delta t(\mu\text{s})$	$1/\delta t$	#Cells Model B	#Cells Model A
128	29.0044	34 477	208 130	81 516
64	7.2511	137 910	1 751 495	714 128
48	4.0787	245 176	4 206 178	1 730 890
32	1.8128	551 633	14 366 575	5 967 144
16	0.4532	2 206 531	116 370 643	48 787 963
8	0.1133	8 826 125	929 916 251	394 432 233

Table 1: Spatial and temporal discretization of the models and corresponding number of fluid cells

The simulations were performed on the *SuperMUC*¹ petascale system, which is a tier-0 PRACE² supercomputer installed at the Leibniz Supercomputing Center, Munich. The *SuperMUC* is one of the main federal compute resources in Germany and it is ranked among the top 20 supercomputers of the world³. *Musubi* exhibits an optimal scaling when the number of cells per core ranges from 2000 to 1 million²⁶; we accordingly regulated

¹<http://www.lrz.de/english/>

²<http://www.prace-ri.eu>

³<http://www.top500.org>

the number of used cores for an efficient utilization of the compute resources and this ranged from 64 to 16384.

2.2 Flow characterization

The assessment of grid convergence was done in a different manner for Models A and B, due to the respective laminar and transitional flow regime. For the Model A, arithmetic average of the global quantities (velocity and WSS) was calculated at 6 planes (see Figure 1) after the simulation achieved a steady state i.e. there was no change in velocity and WSS due to initial fluctuations anymore. These quantities at $8\ \mu m$ were taken as a reference solution and relative percentage errors were then computed for solutions at each coarser resolution with respect to the reference solution as:

$$\delta = \left| \frac{U_{ref} - U_h}{U_{ref}} \right| \times 100 \quad (1)$$

where U_{ref} denotes the reference solution and U_h denotes the solution at coarser resolutions.

Due to the presence of transitional flow in Model B, the flow field was simulated up to a total of $n=8$ seconds in order to obtain reasonable statistics and quantify turbulent characteristics of the flow. Point probes were placed at 10 different locations inside the aneurysm dome and the probe with maximum strain rate and fluctuations was used for the analysis presented here. The instantaneous three-dimensional velocity fields inside the aneurysm dome were decomposed into a mean and a fluctuating part i.e.

$$u_i(\mathbf{x}, t) = \bar{u}_i(\mathbf{x}) + u'_i(\mathbf{x}, t) \quad (2)$$

The mean velocity (\bar{u}_i) is the time averaged velocity over last $n=6$ seconds obtained using the Ergodic theorem.

The Turbulent Kinetic Energy (TKE) was derived from the fluctuating components of the velocity as

$$k = \frac{1}{2} \left(u_x'^2 + u_y'^2 + u_z'^2 \right) \quad (3)$$

The Fourier transform of the TKE was computed to obtain power spectra and to quantify the changes brought by each refinement. The period of the Fourier transform was equal to $n=6$ seconds.

The Q-criterion

The Q-criterion was preferred in the present study for the visualization of coherent flow structures as it shares properties with both the vorticity and pressure criterion¹⁹. The Q-criterion is the second invariant of the velocity gradient tensor $\nabla \mathbf{u}$, and reads:

$$Q = \frac{1}{2} (\Omega_{ij} \Omega_{ij} - S_{ij} S_{ij}) \quad (4)$$

where

$$\Omega_{ij} = \frac{1}{2} \left(\frac{\partial u_i}{\partial x_j} - \frac{\partial u_j}{\partial x_i} \right) \quad (5)$$

and

$$S_{ij} = \frac{1}{2} \left(\frac{\partial u_i}{\partial x_j} + \frac{\partial u_j}{\partial x_i} \right) \quad (6)$$

are respectively the anti-symmetric and symmetric components of $\nabla \mathbf{u}$.

The Q-criterion can be physically viewed as the balance between the rotation rate $\Omega^2 = \Omega_{ij}\Omega_{ij}$ and the strain rate $S^2 = S_{ij}S_{ij}$. Positive Q isosurfaces confine the areas where the strength of rotation overcomes the strain - making those surfaces eligible as vortex envelopes. Several interpretations of Q-criterion have been proposed, see for example⁴² which recasts Q in a form which relates to the vorticity modulus ω :

$$Q = \frac{1}{4}(\omega^2 - 2S_{ij}S_{ij}). \quad (7)$$

This implies that the Q is expected to remain positive in the core of the vortex as vorticity increases as the center of the vortex is approached.

Kolmogorov Microscales

The Kolmogorov microscales are the smallest spatial and temporal scales that can exist in a turbulent flow. Viscosity dominates and the TKE is dissipated into heat at the Kolmogorov scale^{10;37}. The Kolmogorov scales are generally described in terms of rate of dissipation of the turbulent kinetic energy per unit mass written as:

$$\epsilon = 2\nu \langle s_{ij}s_{ij} \rangle \quad (8)$$

where ν is the kinematic viscosity and $\|s\| = \sqrt{2s_{ij}s_{ij}}$ and s_{ij} represents the fluctuating rate of strain tensor obtained by replacing u_i and u_j by u'_i and u'_j respectively in equation 6.

Kolmogorov length, time and velocity scales based on ϵ are respectively defined as: $\eta = (\nu^3/\epsilon)^{1/4}$, $\tau_\eta = (\nu/\epsilon)^{1/2}$ and $u_\eta = (\nu\epsilon)^{1/4}$. The presence of powers of 1/4 and 3 however makes these computations prone to truncation errors. We thus define the Kolmogorov microscales in terms of local friction velocity u_* which rewrites the shear stress in units of velocity and thus relates shear between layers of flow, and reads:

$$u_* = \sqrt{\nu\|s\|} \quad (9)$$

From eqs. 8 & 9 and simple algebraic manipulation, the Kolmogorov scales can be deduced in terms of u_* as $\eta = \nu/u_*$, $\tau_\eta = \nu/u_*^2$ and $u_\eta = u_*$.

The quality of the spatial and temporal resolutions δx & δt in simulation is estimated by evaluating their ratio against corresponding Kolmogorov scales i.e.

$$l^+ = \frac{u_*\delta x}{\nu}. \quad (10)$$

and

$$t^+ = \frac{u_*^2\delta t}{\nu} \quad (11)$$

Transition threshold

To explore the *transition threshold* i.e. the critical Re at which the flow transits from laminar regime to the one that exhibits high frequency fluctuations, we performed simulations at varying Reynolds numbers between $Re = 200$ and 300 in steps of $\delta Re = 10$ in Model B. In addition, to examine if any transition would occur in Model A within a physiologically reasonable Re , we performed simulations up to a Reynolds of 650 . These simulations were performed at resolution of $32\mu m$.

3 Results

The flow regime remained laminar and transitional in Model A and B respectively, which is consistent with⁵¹. Flow characteristics of Models A and B are scrutinized with changing refinements in the following. The Kolmogorov microscales and transition threshold are subsequently presented.

3.1 Model A

Velocity field across a slice in the middle of the dome is shown in Figure 2, whereas the Q -Isosurfaces ($Q = 0.6$) inside the dome of Model A at resolutions of $128, 64, 48, 32, 16$ and $8\mu m$ are shown in Figure 3. The main flow is captured at all the resolutions but

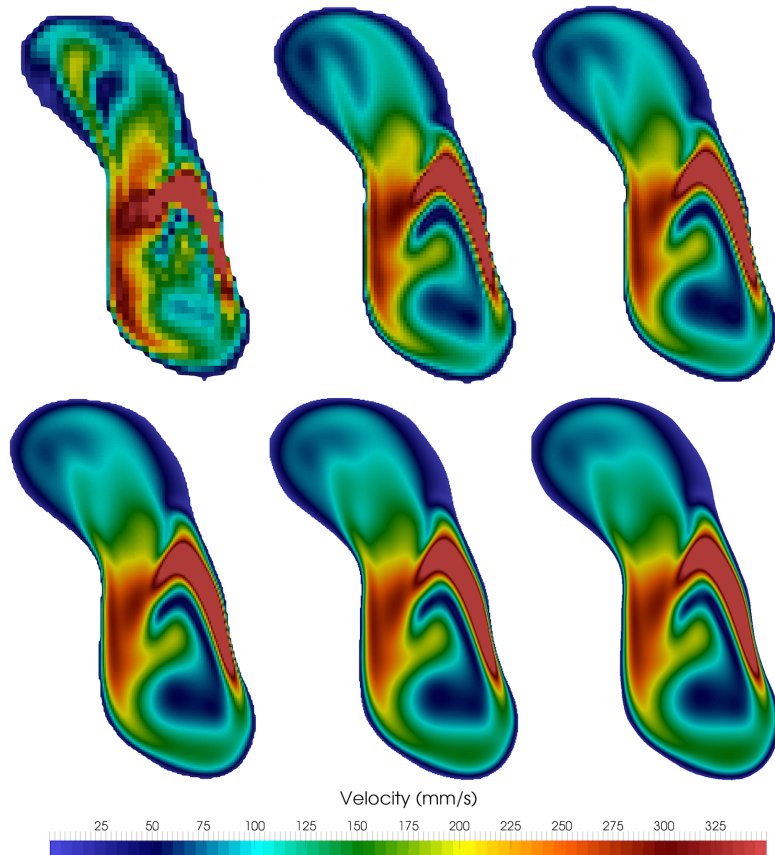


Figure 2: Velocity field across a slice in the middle of the dome of Model A at resolutions of $128, 64, 48$ (L-R top row), $32, 16$ and $8\mu m$ (L-R bottom row).

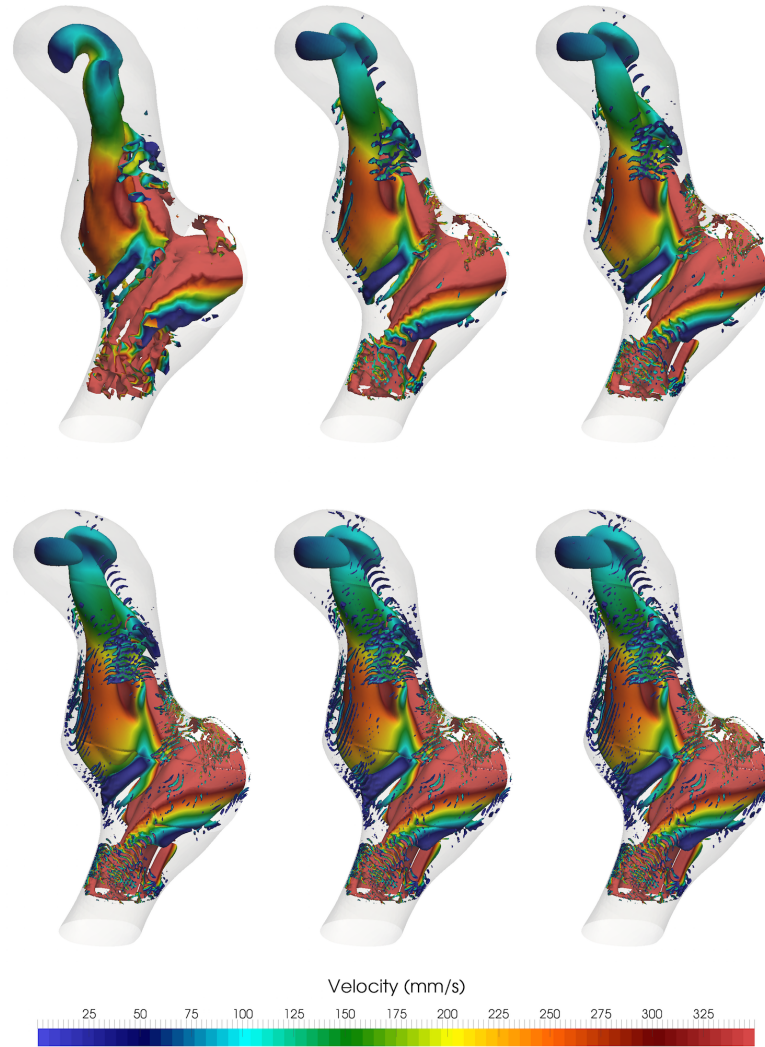


Figure 3: Velocity colored Q-Isosurfaces ($Q=0.6$) at resolutions of 128, 64, 48 (L-R top row), 32, 16 and 8 μm (L-R bottom row).

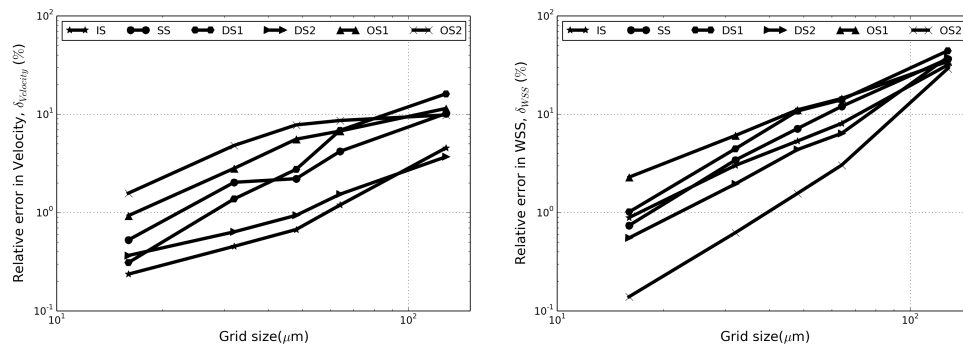


Figure 4: Relative errors in velocity and WSS at resolutions of 128, 64, 48, 32 and 16 μm with respect to reference solution at 8 μm

128 μm is under-resolved as can be seen, e.g., near the top of the aneurysm sac. The flow and the vortices appear similar at 32, 16 and 8 μm .

Figure 4 shows the relative errors in velocity and WSS for solutions at each resolution

in different slices against the reference solution at finest resolution. Errors between 28 and 45% are observed in WSS at coarsest resolution of $128\ \mu\text{m}$ at all the slices, which decreases to less than 15% at $64\ \mu\text{m}$. The effective rate of convergence is ~ 2 at resolutions coarser than $64\ \mu\text{m}$ and ~ 1.5 at resolutions finer than $48\ \mu\text{m}$. The error remains below 2% at all the locations for $16\ \mu\text{m}$. The rate of change from 32 to $16\ \mu\text{m}$ is less than 1% for OS2 and DS2 whereas at other slices this rate is as much as up to $\sim 4\%$.

The errors in velocity in the range of 2 – 16% are comparatively lesser than those in WSS. An *oscillatory* behavior can be observed with respect to the rate of change in these errors at various slices which assumes a nearly 1.5 order after $48\ \mu\text{m}$. Like WSS, errors in velocity are also just less than 2% at $16\ \mu\text{m}$.

3.2 Model B

Velocity field at a slice in the middle of the dome of model B is shown in figure 5 at $t=8\ \text{s}$. Whereas instantaneous velocity field can not be compared for transitional flows, the figure is illustrative to depict the capture of fluctuations with refinement. The flow does not reach the top of aneurysm dome for $128\ \mu\text{m}$ and the flow field appears laminar. The velocity field looks chaotic only at resolutions higher than $48\ \mu\text{m}$. Figure 6

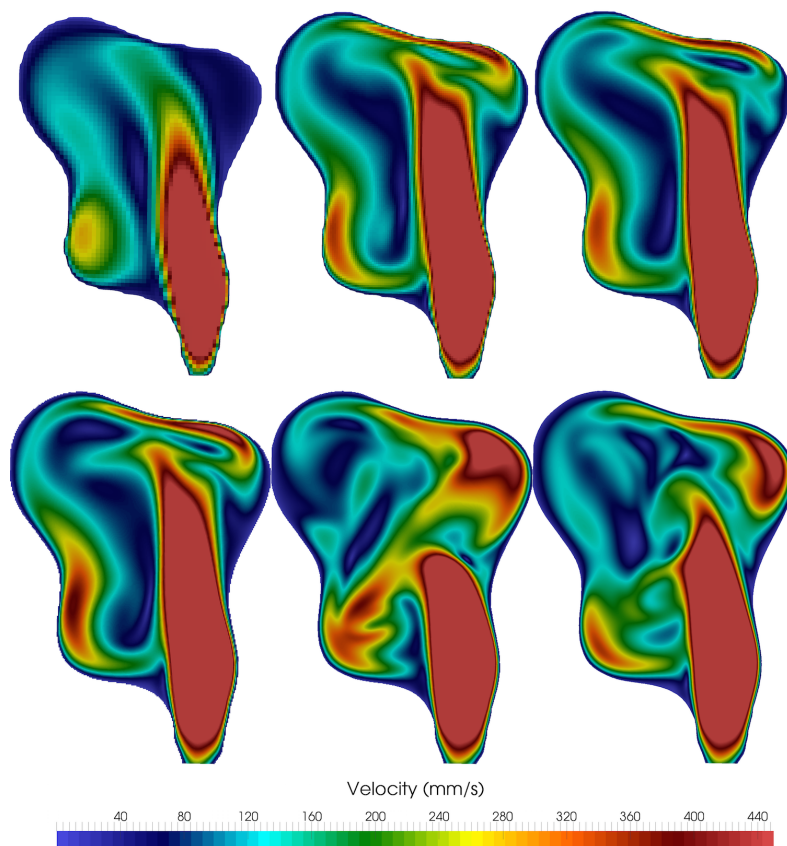


Figure 5: Velocity field across a slice in the middle of the dome of Model B at resolutions of 128, 64, 48 (L-R top row), 32, 16 and $8\ \mu\text{m}$ (L-R bottom row), at the 8th second in the simulation.

shows the Q -isosurfaces ($Q = 0.6$) for each resolution computed as mean of observations at 50 equidistant time intervals between 7th and 8th second of the simulation. The Q -isosurfaces are colored by velocity magnitude and are overlapped with the velocity vectors. Successive refinements result in addition of vortices. At the higher resolutions

of 32, 16 and $8\ \mu\text{m}$, miniature *near wall vortices* are educed by the Q-isosurfaces. The main difference between 16 & $8\ \mu\text{m}$ is additional vortices near the walls and a minor shift in the velocity vectors at $8\ \mu\text{m}$. The flow fluctuations in Model B are depicted in Figure

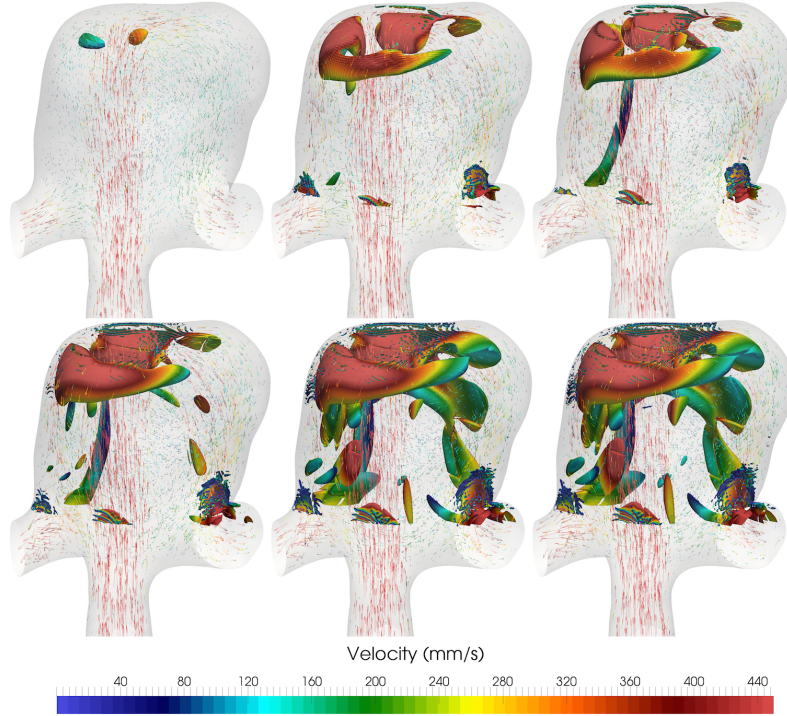


Figure 6: Velocity colored Q-isosurfaces ($Q = 0.6$) inside the dome of Model B at resolutions of 128, 64, 48 (L-R top row), 32, 16 and $8\ \mu\text{m}$ (L-R bottom row) computed as mean between 7th and 8th second of the simulation.

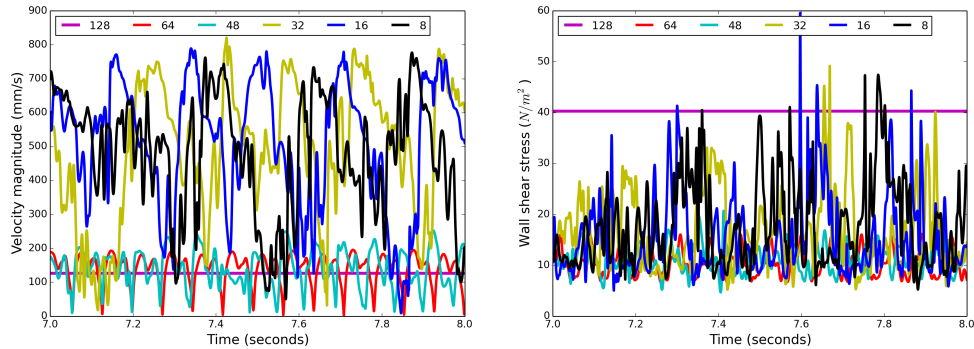


Figure 7: Velocity (L) and WSS (R) fluctuations inside the dome of Model B at various grid resolutions, shown between 7th and 8th second of the simulation.

7(a) at one point in the center of aneurysm dome for all the resolutions, over a time span of one second in the simulation. The flow at the coarsest resolution of $128\ \mu\text{m}$ appears to be laminar with velocity less than $200\ \text{mm/s}$. The same was discovered for flow at other points and slices in the aneurysm at this resolution. The minor smooth and periodic flow instabilities (u') for resolutions of 64 and $48\ \mu\text{m}$ are less than $200\ \text{mm/s}$. However, at higher resolutions, the flow transitions from a laminar regime, and u' increases to $\sim 600\ \text{mm/s}$, yet with a phase difference between flows at all higher resolutions. A similar behavior is observed for the magnitude of WSS which is shown in Figure 7(b).

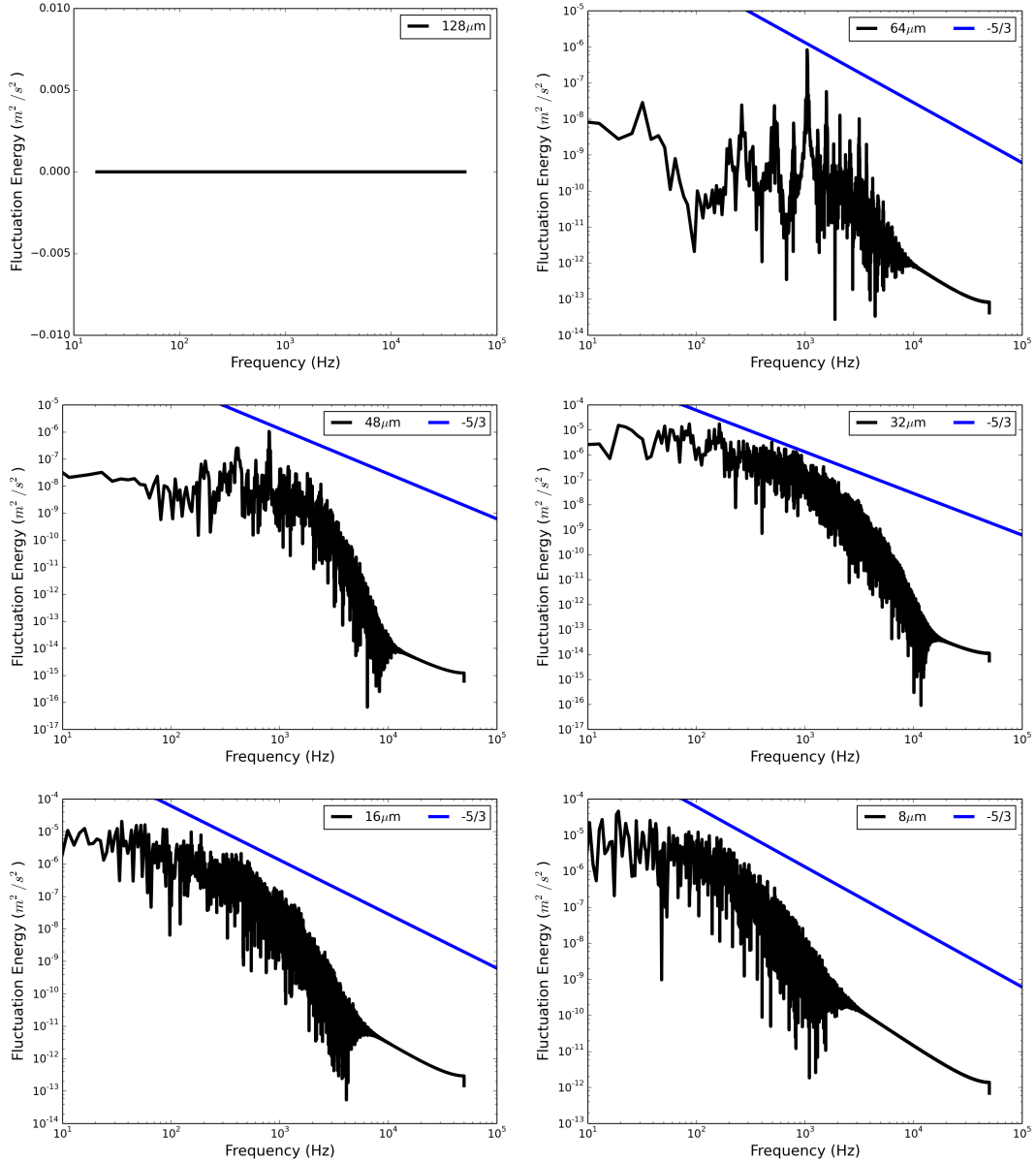


Figure 8: Maps of the Turbulent Kinetic Energy for resolutions of 128, 64, 48, 32, 16 and $8 \mu m$ respectively at a point inside the center of dome of Model B.

The TKE spectra for each resolution is shown in Figure 8 where an increase in the frequency of oscillations with refinements can be observed. A reference line represents the Kolmogorov $-5/3$ energy decay for a comparison with the obtained TKE spectra¹⁰. No spectrum is seen at $128 \mu m$. The spectrum at $64 \mu m$ has irregularity in the peaks, which starts to vanish upon further refinements. From 32 to $8 \mu m$, an observable change is in the shift of decaying zone to the left. This shift is much less from 16 to $8 \mu m$ and there is no mode below a fluctuation energy of 10^{-14} . The behavior of the TKE spectra is weakly similar to the Kolmogorov $-5/3$ decay. This observation is similar to what was seen in the Q-isosurfaces and suggests that the flow is not fully developed turbulence but is in a transitional regime.

$\delta x(\mu\text{m})$	$\delta t(\mu\text{s})$	l^+	t^+	$\eta(\mu\text{m})$	$\tau_\eta(\mu\text{s})$	$u_\eta(\text{mm/s})$
64	7.25	2.75	0.0048	23.30	1510.0	39.58
48	4.07	1.54	0.0035	31.18	1160.0	41.04
32	1.81	0.89	0.0018	36.20	1010.0	89.86
16	0.45	0.41	0.0010	38.90	430.0	96.62
8	0.11	0.27	0.0004	28.80	230.17	121.52

Table 2: The ratio of spatio-temporal scales (l^+, t^+) in the simulation and the Kolmogorov microscales for different resolutions.

Kolmogorov Microscales

Table 2 lists the Kolmogorov microscales for each resolution ⁴. The quantities in table 2 are computed as temporal average between 7&8 seconds in the simulation. t^+ is much lower than 1 at all the resolutions, due to the intrinsically small δt in LBM simulations. The l^+ is ~ 1 for $32\mu\text{m}$ and remains below 1 for spatial resolutions higher than $32\mu\text{m}$. It should be noted that l^+, t^+ and u_η are local quantities and are expected to vary at each computational cell. Therefore table 2 depicts these quantities at the probe where friction velocity was found to be maximum.

3.3 Transition threshold

The flow remained stationary in Model B for Re upto ~ 220 . Minor periodic fluctuations developed at $Re = 250$, the amplitude of which grew up to 300. Phase spectrum of TKE for 3 different Re is shown in Figure 9 along with that for $Re = 351$, at which refinement study was conducted. The fluctuations at $Re = 300$ are of the order of ~ 60 Hz. The Re of 351 thus seems to be near to the critical Re . Flow in model A was simulated up to

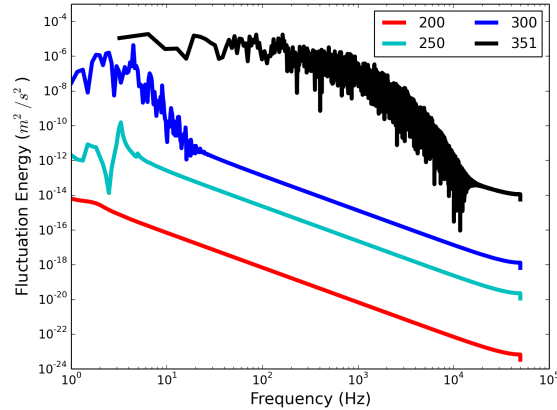


Figure 9: TKE maps at 4 different Reynolds numbers of 200, 250, 300 and 351. Low frequencies of up to 10 Hz are seen for 250 which increase to about 60 Hz for $Re = 300$. Plot shows results at $\delta x = 32\mu\text{m}$

$Re = 650$, and it remained stable with no fluctuations in any part of the model.

⁴Note that Kolmogorov microscales at $128\mu\text{m}$ are not shown because that resolution depicts the flow as laminar and hence computes nearly 0 friction velocity thereby providing misleading information about the turbulent scales.

4 Discussion

The results of our present simulations, which were very highly resolved in space and time, have confirmed that some intracranial aneurysms promote transition inside the dome and it seems that high resolutions simulations are required to capture the transition. The coarsest resolution ($128 \mu m$) was incapable of detecting any transition in the aneurysm, but the considerably higher resolutions ($16,8 \mu m$) on the other hand exposed intricate vortices.

Transitional flow in aneurysms - analysis and significance

The low Re in the parent artery of aneurysms has propelled the assumption of laminar flow in aneurysms - an assumption that advocates the choice of resolution and accuracy in a simulation. Evidence on the presence of high-frequency flow fluctuations in aneurysms however exists, both in clinical and experimental studies^{12;40;54}. This has not been properly addressed in computational studies, except for a few recent publications^{50;51;52}.

The Q-isosurfaces (Fig. 6) indicated that the flow in Model B became transitional after the inflow jet collided with the upper aneurysmal wall, giving rise to coherent structures in the bulk flow and minuscule vortex envelopes near the walls. The impact of inflow jet in Model A was restricted to just over the aneurysmal sac thereby inhibiting the flow from becoming transitional. At a first glance the small vortices which appeared near the walls of Model A give an impression of transition; it should however be observed that the magnitude of velocity across these vortices was minimal whereas it was maximal across near-wall vortices in Model B.

The appearance of near wall vortices in aneurysms has ostensibly a potential role in understanding of turbulence induced wall-degradation, complex process like mechanotransduction⁸, and consequently aneurysm rupture. The role of turbulent flow in increasing thrombosis has been previously studied in which they report the weight of thrombosis as proportional to the Reynolds number and turbulence intensity⁴⁷.

The critical Re for Model B was at the border of Re at which the simulation was conducted (351), suggesting the occurrence of transition in aneurysms at the peak systolic conditions of the MCA M1 segment²⁷. The flow is expected to destabilize during deceleration as was shown in⁵⁰ whereas acceleration is expected to re-laminarize the flow³⁶ - the critical Re thus explored with constant inflow in this study is ostensibly higher than a simulation with pulsatile flow²¹. Insight into critical Re is even more significant when the variability of the heart rate is taken into account like that in,²² and the changes in heart rate are expected to give rise to intriguing vortical structures in the flow.

The classification of a bifurcation aneurysm as an initiator of transition is further supported by the fact that no transition occurred in Model A upon doubling the parent artery Reynolds number (to 650), which is an upper limit for a physiologically reasonable Re . Moreover, the fluctuations were confined to the aneurysm dome for all refinements of Model B and did not occur in other parts of the vasculature under study, which characterizes the manifestation of aneurysm itself as an initiator of fluctuations.

Numerical method and resolutions

LBM is an alternative technique for the numerical solution of the Navier-Stokes equations. Under the continuum limits of low *Mach* and *Knudsen* numbers, the Lattice Boltzmann

equation converges to the Navier-Stokes equations²⁴. The LBM due to a very strict control of numerical viscosity allows for an efficient Direct Numerical Simulation (DNS) of transitional flows at moderate Reynolds numbers^{24;39}. Moreover, the LBM has relatively low numerical dissipation even at the scales of grid spacing as well as small numerical dispersive effects^{29;30}, which are less than what is observed in conventional CFD methods of similar (second-order) accuracy³³. Also, the isotropic nature of LBM ensures the conservation of angular momentum (vorticity) numerically. Several comparisons of LBM with classical CFD techniques exist in literature, of which^{14;2;33} are exemplarily mentioned here.

In the present space-time refinement study, the δt was refined as a consequence of refined δx to follow the diffusive time scaling. The δt thus obtained in these simulations can not be directly enforced to a regular simulation because LBM is not very sensitive to the choice of δt from the point of view of numerical stability. The relaxation parameter Ω can be fine-tuned to obtain similar solutions at impressively larger values of δt . Furthermore, a stencil with higher number of discrete velocity directions(e.g. D3Q27) could have been chosen for LBM computations but it has been shown that the increase in accuracy for moderate Re flows is not phenomenal with larger stencils though the memory requirement increases considerably³⁵. For further details about the coupling of δx and δt , we refer the reader to^{31;39}.

The results of the present study were surprisingly never *converged* in the classical sense⁴¹ as errors in Model A did not attain machine precision (zero), and the phase spectrum was never super-imposable for two successive resolutions of Model B. The error drop from 32 to 16 μm was miniature for Model A and the Q-isosurfaces for both Model A and B displayed a *qualitatively* similar behavior, which gives content in accepting the solutions at these resolutions as similar. The l^+ and t^+ depicted the scales of current simulations as sufficient to resolve the smallest structures in the flow field. At resolutions higher than 32 μm , l^+ was < 1 implying the capture of every possible spatial structure that might appear inside the aneurysms. The small l^+ and t^+ for all the resolutions was a consequence of low friction velocity which is dependent on the Reynolds number. Moreover, the coarse resolutions computed a lower (and inaccurate) u_* resulting in lower values of l^+ and t^+ .

The present results would thus uphold that a δx ranging from 16 to 32 μm is a reasonable choice for simulating aneurysm hemodynamics with LBM. Another implication however is that every aneurysm might require its own convergence analysis as evident from the differences in Model A and B. This observation is also largely consistent with¹⁸. The recommendations from this study can not be extrapolated to other discretization techniques, and whether this resolution requirement applies to other methods warrants a detailed application specific comparison, not performed so far in the context of transitional flows in aneurysms to the authors' knowledge.

Assumptions, limitations and the continuum hypothesis

A uniform velocity at the inlet leads to negligence of secondary flow patterns produced by the upstream vessel curvature and the internal carotid artery bifurcation. These patterns might affect the aneurysmal flow and its stability. Nonetheless the use of a steady flow at peak systolic conditions was a reasonable choice to isolate the sum of geometrical factors that promote high-frequency velocity fluctuations. Velocity fluctuations could cause loss of coherence in bulk flow pattern as the flow begins to decelerate, and in the absence of

a patient specific flow profile, it would have been hard to generalize these results.

Blood does not behave as a Newtonian fluid due to the suspension of red blood cells (RBC), platelets and plasma. For the present study, the assumption of blood as a Newtonian fluid was considered appropriate since previous research has indicated that the aneurysm morphology has a much more pronounced influence on the flow regime than the non-Newtonian behavior of underlying flow¹³, and the choice of Newtonian description of blood has been demonstrated to be somewhat reasonable under the assumption of laminar flow¹¹. Computational models have shown very little effect of the wall deformation on the main flow patterns⁵⁵. Both non-linear viscosity and the fluid-structure interaction may have stabilizing or de-stabilizing effects on the flow. For instance, in arteriovenous grafts turbulence induced wall vibration has been found *in vivo*, but is not observed in Newtonian flow simulations within rigid vessels⁴⁵. The near-wall vortices, which were a major finding of this study are however expected to change with wall deformation. It can however be contended that the qualitative behavior of the eduction of vortices with refinements is less likely to differ.

Under the assumption of blood as a Newtonian fluid, the highest spatial discretization in our simulations was $\delta x = 8 \mu m$, which is comparable to the size of RBCs. At these and probably higher spatial scales, blood can not be treated as a continuum and should be modeled as a suspension. It has been hypothesized¹ that the RBC-RBC interactions would obviate the formation of eddies down to the Kolmogorov scales and it remains questionable whether the miniature vortices reported in this study would actually form in real biological flows. As discussed above the goal of this study was to identify numerical convergence by performing simulations up to the computational limits. The role of RBC interactions can not be unequivocally stated in the absence of appropriate models and experimental data and we contend that RBC role is inconceivable when the blood is predominantly assumed as a Newtonian fluid - a presumption that advocates the choice of resolutions as in the present study for accurate numerical results. Lattice Boltzmann model for blood at mesoscale demonstrated in⁴⁸ would be more appropriate for simulations at these scales, and motivates the use of LBM.

5 Conclusions

The study confirms the presence of transitional flow in aneurysms under the simplified modeling assumptions using highly resolved Lattice Boltzmann simulations. The Kolmogorov scales were of the order of $\sim 29 \mu m$, $230 \mu s$ and $121 mm/s$ for finest resolutions. The occurrence of transition was aneurysm-specific as the model B showed fluctuations already at $Re=250$ while the model A had none up to $Re=650$. Critical Re for transition in model B was ~ 350 whereas model A did not promote any transition within a physiologically reasonable range of Re .

Conflict of Interest

None of the authors have any conflict of interest to report.

Acknowledgements

We are thankful to the Leibniz Supercomputing Center, Munich for providing compute resources (Grant ID: pr85mu) required for this research, and for their kind support. This work has been supported by the Research Council of Norway through grant no. 209951 and a Center of Excellence grant awarded to the Center for Biomedical Computing at Simula Research Laboratory.

References

- ¹ ANTIGA, L., AND STEINMAN, D. A. Rethinking turbulence in blood. *Biorheology* 46, 2 (2009), 77–81.
- ² AXNER, L., HOEKSTRA, A. G., JEAYS, A., LAWFORD, P., HOSE, R., AND SLOOT, P. M. Simulations of time harmonic blood flow in the mesenteric artery: comparing finite element and lattice boltzmann methods. *Biomedical engineering online* 8, 1 (2009), 23.
- ³ BOUZIDI, M., FIRDAOUSS, M., AND LALLEMAND, P. Momentum transfer of a boltzmann-lattice fluid with boundaries. *Physics of Fluids* 13 (2001), 3452.
- ⁴ BYRNE, G., AND CEBRAL, J. Vortex dynamics in cerebral aneurysms. *arXiv preprint arXiv:1309.7875* (2013).
- ⁵ CEBRAL, J. R., MUT, F., WEIR, J., AND PUTMAN, C. Quantitative characterization of the hemodynamic environment in ruptured and unruptured brain aneurysms. *American Journal of Neuroradiology* 32, 1 (2011), 145–151.
- ⁶ CEBRAL, J. R., MUT, F., WEIR, J., AND PUTMAN, C. M. Association of hemodynamic characteristics and cerebral aneurysm rupture. *American Journal of Neuroradiology* 32, 2 (2011), 264–270.
- ⁷ CHNAFA, C., MENDEZ, S., AND NICLOUD, F. Image-based large-eddy simulation in a realistic left heart. *Computers & Fluids* 94 (2014), 173–187.
- ⁸ DAVIES, P. F., REMUZZI, A., GORDON, E. J., DEWEY, C. F., AND GIMBRONE, M. A. Turbulent fluid shear stress induces vascular endothelial cell turnover in vitro. *Proceedings of the National Academy of Sciences* 83, 7 (1986), 2114–2117.
- ⁹ DI CARLO, A. Human and economic burden of stroke. *Age and ageing* 38, 1 (2009), 4–5.
- ¹⁰ DURBIN, P. A., AND REIF, B. P. *Statistical theory and modeling for turbulent flows*. John Wiley & Sons, 2011.
- ¹¹ EVJU, Ø., VALEN-SENDSTAD, K., AND MARDAL, K.-A. A study of wall shear stress in 12 aneurysms with respect to different viscosity models and flow conditions. *Journal of biomechanics* 46, 16 (2013), 2802–2808.
- ¹² FERGUSON, G. G. Turbulence in human intracranial saccular aneurysms. *Journal of neurosurgery* 33, 5 (1970), 485–497.

- ¹³ FISHER, C., AND ROSSMANN, J. S. Effect of non-newtonian behavior on hemodynamics of cerebral aneurysms. *Journal of biomechanical engineering* 131, 9 (2009), 091004.
- ¹⁴ GELLER, S., KRAFCZYK, M., TÖLKE, J., TUREK, S., AND HRON, J. Benchmark computations based on lattice-boltzmann, finite element and finite volume methods for laminar flows. *Computers & Fluids* 35, 8 (2006), 888–897.
- ¹⁵ HARLACHER, D. F., HASERT, M., KLIMACH, H., ZIMNY, S., AND ROLLER, S. Tree based voxelization of stl Data. In *High Performance Computing on Vector Systems 2011*, M. Resch, X. Wang, W. Bez, E. Focht, H. Kobayashi, and S. Roller, Eds. Springer Berlin Heidelberg, 2012, pp. 81–92.
- ¹⁶ HASERT, M. *Multi-scale Lattice Boltzmann simulations on distributed octrees*. PhD thesis, Aachen, Techn. Hochsch., Diss., 2013, 2014.
- ¹⁷ HASERT, M., MASILAMANI, K., ZIMNY, S., KLIMACH, H., QI, J., BERNSDORF, J., AND ROLLER, S. Complex fluid simulations with the parallel tree-based lattice boltzmann solver musubi. *Journal of Computational Science* (2013).
- ¹⁸ HODIS, S., UTHAMARAJ, S., SMITH, A. L., DENNIS, K. D., KALLMES, D. F., AND DRAGOMIR-DAESCU, D. Grid convergence errors in hemodynamic solution of patient-specific cerebral aneurysms. *Journal of biomechanics* 45, 16 (2012), 2907–2913.
- ¹⁹ HUNT, J. C., WRAY, A., AND MOIN, P. Eddies, streams, and convergence zones in turbulent flows. In *Studying Turbulence Using Numerical Simulation Databases, 2* (1988), vol. 1, pp. 193–208.
- ²⁰ JAIN, K. Direct numerical simulation of transitional pulsatile stenotic flow using lattice boltzmann method. *PeerJ PrePrints* 3 (11 2015), e1928.
- ²¹ JAIN, K., AND MARDAL, K.-A. Exploring the critical reynolds number for transition in intracranial aneurysms - highly resolved simulations below kolmogorov scales. 560 – 563. 2015 Computational and Mathematical Biomedical Engineering.
- ²² JIANG, J., AND STROTHER, C. Computational fluid dynamics simulations of intracranial aneurysms at varying heart rates: a patient-specific study. *Journal of biomechanical engineering* 131, 9 (2009), 091001.
- ²³ JOHANNINK, M., MASILAMANI, K., MHAMDI, A., ROLLER, S., AND MARQUARDT, W. Predictive pressure drop models for membrane channels with non-woven and woven spacers. *Desalination* 376 (2015), 41–54.
- ²⁴ JUNK, M., KLAR, A., AND LUO, L.-S. Asymptotic analysis of the lattice boltzmann equation. *Journal of Computational Physics* 210, 2 (2005), 676–704.
- ²⁵ JUNK, M., AND YANG, Z. Asymptotic Analysis of Lattice Boltzmann Outflow Treatments. *Communications in Computational Physics* (2011), 1–11.
- ²⁶ KLIMACH, H., JAIN, K., AND ROLLER, S. End-to-end parallel simulations with apes. In *Parallel Computing: Accelerating Computational Science and Engineering (CSE)* (Munich, Germany, September 2014), M. Bader, A. Bode, H.-J. Bungartz, M. Gerndt,

- G. R. Joubert, and F. Peters, Eds., vol. 25 of *Advances in Parallel Computing*, IOS Press, pp. 703–711.
- ²⁷ KREJZA, J., SZYDLIK, P., LIEBESKIND, D. S., KOCHANOWICZ, J., BRONOV, O., MARIAK, Z., AND MELHEM, E. R. Age and sex variability and normal reference values for the vmca/vica index. *American journal of neuroradiology* 26, 4 (2005), 730–735.
- ²⁸ KRÜGER, T., VARNIK, F., AND RAABE, D. Shear stress in lattice Boltzmann simulations. *Physical Review E* 79, 4 (Dec. 2008), 15.
- ²⁹ LALLEMAND, P., AND LUO, L.-S. Theory of the lattice boltzmann method: Dispersion, dissipation, isotropy, galilean invariance, and stability. *Physical Review E* 61, 6 (2000), 6546.
- ³⁰ LALLEMAND, P., AND LUO, L.-S. Theory of the lattice boltzmann method: Acoustic and thermal properties in two and three dimensions. *Physical review E* 68, 3 (2003), 036706.
- ³¹ LATT, J. *Hydrodynamic limit of lattice Boltzmann equations*. PhD thesis, University of Geneva, 2007.
- ³² LEE, S. E., LEE, S.-W., FISCHER, P. F., BASSIOUNY, H. S., AND LOTH, F. Direct numerical simulation of transitional flow in a stenosed carotid bifurcation. *Journal of biomechanics* 41, 11 (2008), 2551–2561.
- ³³ MARIÉ, S., RICOT, D., AND SAGAUT, P. Comparison between lattice boltzmann method and navier–stokes high order schemes for computational aeroacoustics. *Journal of Computational Physics* 228, 4 (2009), 1056–1070.
- ³⁴ MIURA, Y., ISHIDA, F., UMEDA, Y., TANEMURA, H., SUZUKI, H., MATSUSHIMA, S., SHIMOSAKA, S., AND TAKI, W. Low wall shear stress is independently associated with the rupture status of middle cerebral artery aneurysms. *Stroke* 44, 2 (2013), 519–521.
- ³⁵ NASH, R. W., CARVER, H. B., BERNABEU, M. O., HETHERINGTON, J., GROEN, D., KRÜGER, T., AND COVENEY, P. V. Choice of boundary condition for lattice-boltzmann simulation of moderate-reynolds-number flow in complex domains. *Physical Review E* 89, 2 (2014), 023303.
- ³⁶ PEACOCK, J., JONES, T., TOCK, C., AND LUTZ, R. The onset of turbulence in physiological pulsatile flow in a straight tube. *Experiments in fluids* 24, 1 (1998), 1–9.
- ³⁷ POPE, S. B. *Turbulent flows*. Cambridge university press, 2000.
- ³⁸ QIAN, Y., TAKAO, H., UMEZU, M., AND MURAYAMA, Y. Risk analysis of unruptured aneurysms using computational fluid dynamics technology: preliminary results. *American Journal of Neuroradiology* 32, 10 (2011), 1948–1955.
- ³⁹ RHEINLÄNDER, M. Analysis of lattice-boltzmann methods.
- ⁴⁰ ROACH, M. R., SCOTT, S., AND FERGUSON, G. G. The hemodynamic importance of the geometry of bifurcations in the circle of willis (glass model studies). *Stroke* 3, 3 (1972), 255–267.

- ⁴¹ ROACHE, P. J. Quantification of uncertainty in computational fluid dynamics. *Annual Review of Fluid Mechanics* 29, 1 (1997), 123–160.
- ⁴² ROBINSON, S. K. The kinematics of turbulent boundary layer structure. *NASA STI/Recon Technical Report N 91* (1991), 26465.
- ⁴³ ROLLER, S., BERNSDORF, J., KLIMACH, H., HASERT, M., HARLACHER, D., CAKIRCALI, M., ZIMNY, S., MASILAMANI, K., DIDINGER, L., AND ZUDROP, J. An adaptable simulation framework based on a linearized octree. In *High Performance Computing on Vector Systems 2011*, M. Resch, X. Wang, W. Bez, E. Focht, H. Kobayashi, and S. Roller, Eds. Springer Berlin Heidelberg, 2012, pp. 93–105.
- ⁴⁴ SEIFERT, V., TROST, H., AND STOLKE, D. Management morbidity and mortality in grade iv and v patients with aneurysmal subarachnoid haemorrhage. *Acta neurochirurgica* 103, 1-2 (1990), 5–10.
- ⁴⁵ SMITH, D. S. *Experimental Investigation of Transition to Turbulence in Arteriovenous Grafts*. ProQuest, 2008.
- ⁴⁶ STEHBENS, W. Turbulence of blood flow. *Experimental Physiology* 44, 1 (1959), 110–117.
- ⁴⁷ STEIN, P. D., AND SABBAAH, H. N. Measured turbulence and its effect on thrombus formation. *Circulation Research* 35, 4 (1974), 608–614.
- ⁴⁸ SUN, C., AND MUNN, L. L. Lattice-boltzmann simulation of blood flow in digitized vessel networks. *Computers & Mathematics with Applications* 55, 7 (2008), 1594–1600.
- ⁴⁹ TAKAO, H., MURAYAMA, Y., OTSUKA, S., QIAN, Y., MOHAMED, A., MASUDA, S., YAMAMOTO, M., AND ABE, T. Hemodynamic differences between unruptured and ruptured intracranial aneurysms during observation. *Stroke* 43, 5 (2012), 1436–1439.
- ⁵⁰ VALEN-SENDSTAD, K., MARDAL, K.-A., MORTENSEN, M., REIF, B. A. P., AND LANGTANGEN, H. P. Direct numerical simulation of transitional flow in a patient-specific intracranial aneurysm. *Journal of Biomechanics* 44, 16 (2011), 2826–2832.
- ⁵¹ VALEN-SENDSTAD, K., MARDAL, K.-A., AND STEINMAN, D. A. High-resolution computational fluid dynamics detects high-frequency velocity fluctuations in bifurcation, but not sidewall, aneurysms of the middle cerebral artery. *Journal of Biomechanics* 18; 46(2) (2013), 402–7.
- ⁵² VALEN-SENDSTAD, K., AND STEINMAN, D. Mind the gap: Impact of computational fluid dynamics solution strategy on prediction of intracranial aneurysm hemodynamics and rupture status indicators. *American Journal of Neuroradiology* (2013).
- ⁵³ XIANG, J., SIDDIQUI, A., AND MENG, H. The effect of inlet waveforms on computational hemodynamics of patient-specific intracranial aneurysms. *Journal of biomechanics* (2014).

- ⁵⁴ YAGI, T., SATO, A., SHINKE, M., TAKAHASHI, S., TOBE, Y., TAKAO, H., MURAYAMA, Y., AND UMEZU, M. Experimental insights into flow impingement in cerebral aneurysm by stereoscopic particle image velocimetry: transition from a laminar regime. *Journal of The Royal Society Interface* 10, 82 (2013), 20121031.
- ⁵⁵ ZHAO, X., RAGHAVAN, M. L., AND LU, J. Characterizing heterogeneous properties of cerebral aneurysms with unknown stress-free geometry: a precursor to in vivo identification. *Transactions of the ASME-K-Journal of Biomechanical Engineering* 133, 5 (2011), 051008.